Temperature-induced Transition from Indirect to Direct Adsorption of Polycyclic Aromatic Hydrocarbons on Quartz: A Combined Theoretical and Experimental Study

Tu Lan,[†,‡,§] Jing Liu,[†] Hongbo Zeng,[*,†] and Tian Tang,[*,‡]

[†]*Department of Chemical and Materials Engineering, University of Alberta, Edmonton, Alberta T6G 1H9, Canada*

[‡]*Department of Mechanical Engineering, University of Alberta, Edmonton, Alberta T6G 1H9, Canada*

[§]*Key Laboratory of Radiation Physics and Technology, Ministry of Education, Institute of Nuclear Science and Technology, Sichuan University, Chengdu 610064, China*

**Corresponding authors:*

Phone: +1-780-492-1044. E-mail: hongbo.zeng@ualberta.ca (H.Z.).

Phone: +1-780-492-5467. E-mail: tian.tang@ualberta.ca (T.T.).

ABSTRACT:

Adsorption of polycyclic aromatic hydrocarbons (PAHs) on mineral surfaces plays an important role in many engineering fields, such as oil recovery and oil sands production. In this work, the adsorption behaviors of a PAH compound, violanthrone-79 (VO-79), on quartz surface were investigated at different temperatures by molecular dynamics (MD) simulation and atomic force microscopy (AFM). Our simulations demonstrated that with rising temperature, the rate of adsorption increased whereas the total amount of stably adsorbed VO-79 molecules hardly changed. On the other hand, the adsorption mode had a strong dependence on the temperature. At 323K, approximately half of the adsorbed VO-79 formed a monolayer with their polyaromatic cores directly contacting and parallel to the quartz surface. The other half were in an aggregated form and adsorbed indirectly, via interaction with directly adsorbed molecules. The polyaromatic cores of VO-79 in the aggregates tend be oriented slant to the surface. A transition from indirect to direct adsorption was observed as temperature increased, and nearly 90% of VO-79 molecules were adsorbed in direct form at 523K. AFM imaging confirmed the observations in the MD simulations, showing smaller and more uniformly distributed VO-79 aggregates adsorbed on the surface with rising temperature. This work provides valuable insights, at the molecular level, into the effect of temperature on the adsorption of PAHs on mineral surfaces.

1. INTRODUCTION

Adsorption of polycyclic aromatic hydrocarbons (PAHs) on mineral surfaces plays a significant role in many important fields, such as environmental science, oil recovery engineering, etc. PAHs are a group of ubiquitous hydrophobic organic compounds, which are of concerns to human health mainly due to their toxicity and suspected carcinogenity.[1] Presence of minerals can contribute crucially to the retention of PAHs in subsurface environments due to their adsorption.[2] In conventional reservoirs, the wettability alteration of mineral surfaces from oil-wet to water-wet through spontaneous imbibition can significantly enhance the oil recovery.[3] However, the adsorption of PAHs, such as asphaltenes present in the petroleum, can alter the surface wettability from water-wet to oil-wet, increasing the difficulties in oil liberation from reservoir rocks and causing fouling in downstream operations.[4-7] Therefore, understanding the adsorption of PAHs on mineral surfaces is of vital importance for controlling the surface properties of minerals in related engineering processes.

Over the past two decades, significant experimental and simulative efforts have been spent on examining PAH adsorption on minerals, most of which focused on asphaltenes. It was found that the adsorption was a multifaceted process sensitive to many system variables, such as PAH concentration,[8-12] type of minerals,[13-16] polarity of solvents,[17-19] salinity,[20-23] humidity,[24,25] and chemical modifications.[26-28] For instance, Dudášová et al.[8] and Saraji et al.[15] characterized the adsorption of asphaltenes from different origins onto multiple solid surfaces including kaolin, calcite, dolomite and quartz. Both monolayer and multilayer adsorption behaviors were observed, which generally occurred at low and high asphaltene concentrations, respectively.[9] Additionally, polarity of the solvent can affect the adsorption modes.[18] In a good solvent (toluene or xylene), the adsorbed asphaltenes were structured as a solvated monolayer,

whereas the adsorption exhibited a transition from a monolayer to a multilayer structure with the progressive addition of a poor solvent (heptane or dodecane). Saraji et al.[22] investigated the asphaltene adsorption from toluene solution onto quartz in the presence of brine films, revealing that the adsorbed amounts decreased at higher salt concentration mainly due to larger repulsive hydration forces that stabilized the thin brine films on the quartz surface. Gonzalez et al.[24] studied the effect of relative humidity on asphaltenes adsorption onto quartz surface. Their results showed that the adsorption was sensitive to surface-adsorbed water, decreasing linearly with the thickness of the interfacial water film, with a 4-fold reduction in adsorption when relative humidity was increased from 0 to 100%.

In addition to the above factors, temperature also plays a key role in PAH adsorption on mineral surfaces, due to its impact on the colloidal state of PAHs.[29-32] It is generally believed that the size of PAH aggregates decreases as temperature rises,[33,34] thus reducing the amount of adsorption.[30,31,35-37] However, there were a few different reports. Acevedo et al.[32] found that the diameter of asphaltene aggregates increased with rising temperature from 423 to 523 K. Other studies demonstrated that the effect of temperature on adsorption was not significant,[38] or even negligible.[14] Furthermore, One reason for the discrepancies in the literature is the lack of critical information on the temperature-dependent adsorption process, adsorption mode and structure, orientation of molecules, etc., which is hard to obtain experimentally.

Molecular dynamics (MD) simulations have been extensively employed to investigate the adsorption of PAHs on liquid interfaces[39-45] and on mineral surfaces,[46-52] providing insights into the dynamic processes at molecular level. Using MD simulations, Wu et al.[46] investigated the adsorption, diffusion and distribution of asphaltene, resin, aromatic and saturate fractions of heavy crude oil on quartz surface, and found that the

van der Waals (vdW) interaction was the main contributor to the adsorption of these components. Zhu et al.[50] studied the adsorption and aqueous extraction of oil contaminants on silica surface with various roughness, which was modelled by different rectangular grooves. Their results demonstrated that the main resistance for oil release from the relatively shallow grooves was the strong intermolecular interactions between the oil molecules orderly stacked inside the grooves. Xiong et al.[51] probed the adsorption on silica surfaces of two types of PAHs with different length of aliphatic side chains. Their results showed enhanced synergetic adsorption of the two PAHs, which was attributed to the π–π stacking and T-stacking between polyaromatic cores, as well as hydrogen bonding between their polar terminal groups and silica. Our previous MD study[49] showed that at 300K, the type of solvent had a great impact on the kinetics of PAH adsorption on quartz surface, but did not change the adsorption modes. The adsorption was driven primarily by vdW forces, accompanied by electrostatics, hydrogen bonding and free energy of solvation. These past MD simulations were all performed at room temperature (~300 K), while no MD studies have investigated PAH adsorption onto mineral surfaces at other, especially under higher, temperature conditions.

In this work, we have performed MD simulations to study the temperature-dependent adsorption of a representative PAH, violanthrone-79 (VO-79), from organic solvents onto quartz surface. The results allow us to address how temperature influences the adsorption process, mode and adsorbed structures. The simulations have been accompanied by experiments using atomic force microscope (AFM) imaging, providing complementary structure characterization of the adsorbed layers.

2. METHODS

2.1. Simulation

The representative PAH model, VO-79 (Figure 1a), consists of a large polyaromatic core (PAC) and two long aliphatic side chains. Most silica surfaces used in experimental adsorption studies contain many hydroxyl groups on the surface,[53] which are known to enable the adsorption of organic and biological molecules.[54,55] As such a hydroxylated monolayer quartz surface (Figure 1b) was chosen as the mineral surface in this study. To reduce the complexity of the model while maintaining the key functional groups for adsorption, the monolayer quartz surface was created with the silanol (Si−OH) groups on one side of the surface and Si−H groups on the other (Figure 1b). The surface silanol density is about 7.2 OH per nm^2, close to the experimental values (8 OH per nm^2 at maximum coverage) reported in a previous work.[56] The organic solvents were represented by heptane and toluene. The topologies for VO-79, quartz surface, heptane, and toluene were generated and validated in our previous work,[45,49,57-60] and directly adopted here.

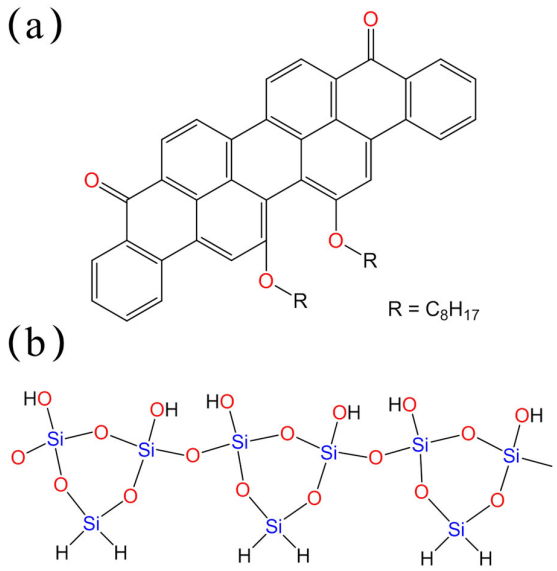

Figure 1. Molecular structures of (a) VO-79 as a PAH model and (b) hydroxylated

quartz surface (side view) employed in this study.

In total, 10 systems were constructed to systematically investigate the VO-79 adsorption on quartz surface at different temperatures. These systems all contained the same number (24) of VO-79 molecules, but having two different types of solvents and 5 different temperatures. Table 1 summarizes the details of the simulated systems, including the number of solvent molecules (N_{heptane} or N_{toluene}), and the temperature (T) at which each system was simulated. Each system was named by the first letter indicating the type of solvent (H for heptane and T for toluene) followed by the value of temperature in Kelvin. For example, system H323 corresponds to simulation of VO-79 adsorption from heptane on quartz at 323K. The initial configuration of each system was built using the procedure reported in our previous work.[49] Briefly, we first constructed a simulation box of 5.7 × 5.6 × 11 nm^3 with 24 VO-79 molecules, which were arranged with their PACs parallel to one another, forming a 4 × 2 × 3 array. The rest of the box was filled with the solvent molecules. An initial steepest descent energy minimization was carried out to ensure that the maximum force was less than 1000.0 kJ/(mol·nm). This procedure was followed by a pre-equilibration with position restraint on the VO-79 molecules in a canonical (*NVT*) ensemble for 100 ps and an isothermal-isobaric (*NPT*) ensemble for another 100 ps. Then, two quartz surfaces were placed on the left and right sides of the box, with the Si–OH groups facing the solvent. The initial configuration of system H323 is shown in Section S1 of the Supporting Information (SI) as an example. After another energy minimization, the system was finally sampled for 100 ns in *NVT* ensemble with position restraint on all silicon atoms of the quartz surfaces.

156 **Table 1.** Details of the Simulated Systems

system	$N_{heptane}$	$N_{toluene}$	T (K)
H323	1331	0	323
H373	1261	0	373
H423	1182	0	423
H473	1085	0	473
H523	1002	0	523
T323	0	1791	323
T373	0	1676	373
T423	0	1560	423
T473	0	1418	473
T523	0	1236	523

157

158 All simulations were performed using the GROMACS 5.0.7 simulation
159 package,[61,62] with periodic boundary conditions applied in all three directions. During
160 all simulations, a time step of 1 fs was used. Temperature was controlled using the
161 v-rescale thermostat,[63] with coupling time (τ_T) set at 0.1 ps. Pressure in *NPT* ensemble
162 was kept at 1 bar by the Parrinello-Rahman barostat,[64] with coupling time (τ_P) set at 2.0
163 ps. The LINCS algorithm was used to constrain all bonds.[65] The particle mesh Ewald
164 (PME) method was applied to handle long-range electrostatic interactions,[66,67] with a
165 Fourier grid spacing of 0.16 nm. A twin-range cutoff scheme was employed for
166 short-range electrostatic and vdW interactions with a cutoff value of 1.4 nm.
167 Appropriate post-processing programs available in GROMACS were used for trajectory
168 analysis and VMD 1.9.1 was applied for visualization.[68]

2.2. Experiment

VO-79 ($C_{50}H_{48}O_4$, 98%), heptane and toluene were purchased from Fisher Scientific. Both heptane and toluene are of HPLC grade. The silica substrate (silicon wafer with 0.5 μm thermal oxide layer) was purchased from the NanoFab, University of Alberta. To conduct the experiment of VO-79 adsorption on silica substrate at different temperatures, VO-79 in heptane and toluene solutions were firstly prepared at the weight concentration of 2000 ppm. Each solution was sonicated in an ultrasound bath for 10 min before being transferred to a hydrothermal reactor. A brief protocol of conducting the VO-79 adsorption on silica substrate is summarized as follows: 1) treating the silica substrate with UV/O_3 to remove any organic contaminants on the substrate surface; 2) immersing the silica substrate in VO-79 solution filled in the hydrothermal reactor and leaving the sealed reactor in a laboratory oven for 1 h at a desired constant temperature; 3) thoroughly rinsing the substrate with the solvent used in the preparation of VO-79 solution in order to remove any weakly adsorbed VO-79, and blow-drying the resultant sample with nitrogen. The surface morphology of adsorbed VO-79 on silica substrate was characterized by atomic force microscope (AFM) imaging in tapping mode operated on a Dimension Icon AFM (Bruker, Santa Barbara, CA). Due to the limitation of the equipment used, the temperatures in the experiments were different from those in the simulations, ranging from 298 to 363 K.

3. RESULTS AND DISCUSSION

3.1. Mode and Rate of Adsorption

The root mean square deviations (RMSD) of VO-79 molecules are plotted as functions of time in Section S2 of SI, which clearly demonstrate the attainment of

equilibrium for all systems in the end. Final equilibrated configurations of the systems are shown in Figure 2. Visual examination of the final structures revealed two modes of adsorption: direct (highlighted by red arrows), where the PACs were parallel to and in direct contact with the quartz surface; and indirect (highlighted by blue circles), where the aggregated VO-79 were adsorbed via the interaction with directly adsorbed molecules. The PACs of VO-79 in the aggregates tend be oriented slant to the surface. In heptane at 323 K and 373 K, all VO-79 were stably adsorbed on the surface without desorption back into the bulk, and both forms of adsorption were present. Stable adsorption was also seen at higher temperature, but more VO-79 molecules exhibited direct adsorption than the indirect form. In contrast, in Figure 2f (T323), one VO-79 molecule preferred to stay in bulk toluene rather than on the surfaces although both adsorption modes were also present. Direct adsorption was found to be dominant at higher temperature in toluene (Figure 2g–2j), and presence of indirect adsorption was not visually apparent. For both solvents, it is clear that the preferred adsorption mode transitioned from indirect to direct form with increasing temperature.

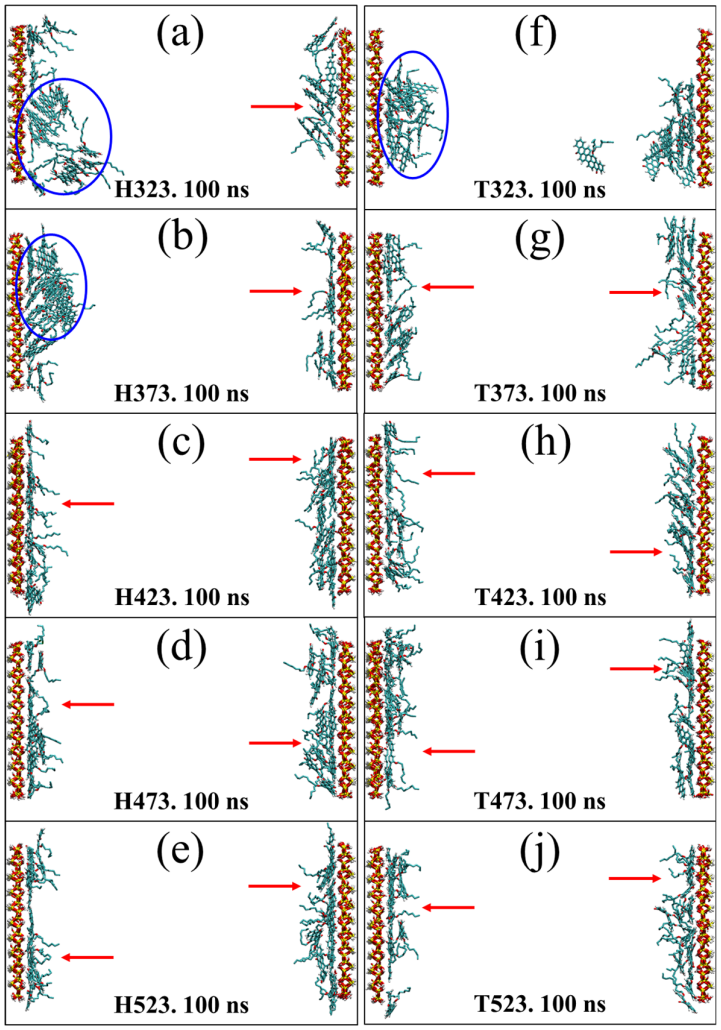

Figure 2. Final configurations of the systems in heptane (left panel): (a) H323, (b) H373, (c) H423, (d) H473 and (e) H523, and in toluene (right panel): (f) T323, (g) T373, (h) T423, (i) T473 and (j) T523. C, H, O, and Si atoms are shown in cyan, white, red, and yellow, respectively. Solvent molecules are not shown for clarity. Blue circles represent the VO-79 molecules adsorbed on the surfaces in the indirect form, whereas red arrows point to the VO-79 molecules with direct adsorption.

The averaged minimum distance between PACs of all VO-79 molecules and quartz surfaces was calculated as a function of time and plotted in Figure 3a–b for all the

systems. The curves show a universal trend of decreasing with time until reaching their equilibrium values. In Figure 3a, for system H323 in heptane, the final equilibrium value (~ 0.5 nm) is significantly larger than the others at higher temperature (~ 0.25 nm). The same phenomenon can be observed in Figure 3b, where higher temperatures lead to smaller equilibrium distance values. In addition, in both plots the curves at 323 and 373 K experience more fluctuations than those at higher temperature before reaching equilibrium. By calculating the minimum distance (d_1) between the PAC of each VO-79 and quartz surface (Section S3 of SI), it was found that for most VO-79 d_1 decreased with time until reaching an equilibrium value of ~ 0.25 nm. This value is close to the distance (0.26 nm) between PACs of adsorbed *N*-(1-hexylheptyl)-*N'*-(5-carboxylicpentyl)-perylene-3,4,9,10-tetracarboxylic bisimide (C5Pe) and silica surface found in a previous study.[48] The distance of 0.25 nm is therefore an indication of adsorption where the VO-79 is in immediate contact with the quartz surface. Based on this, a VO-79 molecule was defined to be in direct adsorption mode if the minimum distance from its PAC to quartz surface was within 0.25 nm.

As mentioned before, some VO-79 were observed to form aggregates, through π-π stacking of their PACs, when they adsorbed on the quartz surface. The minimum separation between stacked PACs of two VO-79 molecules was found to be about 0.35 nm in our previous work.[69] Thus, if a VO-79 molecule had $d_1 > 0.25$ nm (i.e., not directly adsorbed), the minimum distance (d_2) between its PAC and the PACs of all directly adsorbed VO-79 molecules was calculated. If d_2 was no more than 0.35 nm, this VO-79 was regarded as in indirect adsorption ($d_1 > 0.25$ nm and $d_2 \leq 0.35$ nm). Each of

the remaining unclassified VO-79 (with d_1 > 0.25 nm and d_2 > 0.35 nm) was further subjected to minimum distance calculations, between its PAC and the PACs of all indirectly adsorbed VO-79. If the minimum distance was no more than 0.35 nm, then the molecule was also identified as indirectly adsorbed, through one directly adsorbed and another indirectly adsorbed molecule. This process continued until all molecules were classified. The definitions for direct and indirect adsorptions are illustrated in Figure 4.

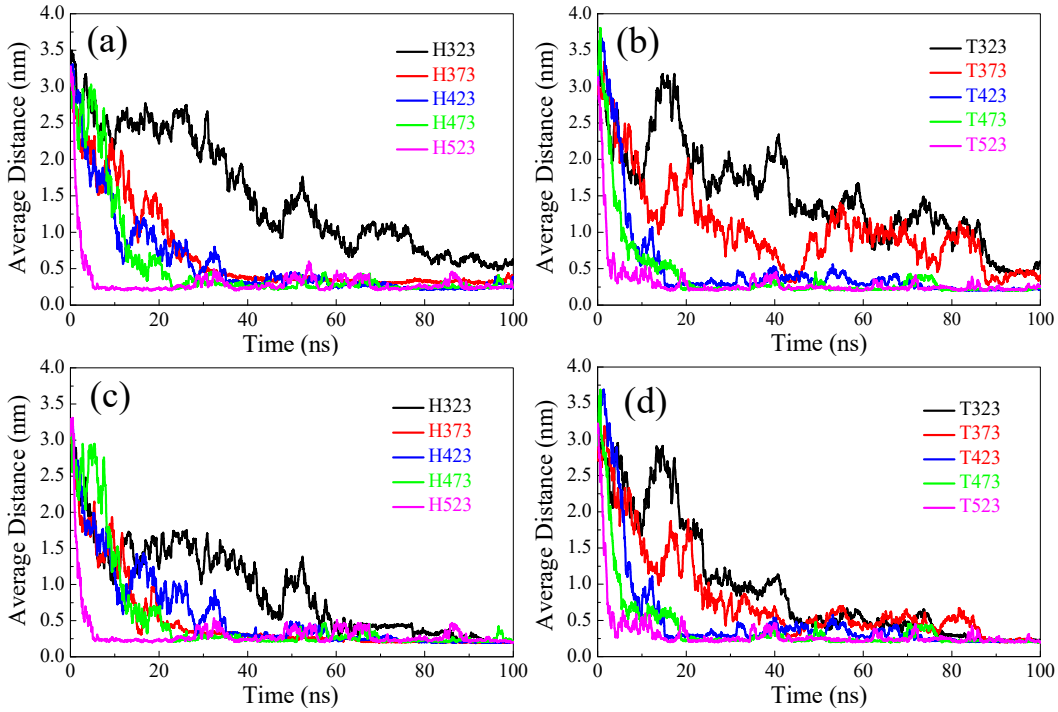

Figure 3. Time evolution of averaged minimum distance between quartz surfaces and the PACs of all VO-79 in systems (a) with heptane as the solvent, (b) with toluene as the solvent. Time evolution of averaged minimum distance between quartz surfaces and the PACs of all directly adsorbed VO-79 in systems (c) with heptane as the solvent, (d) with toluene as the solvent.

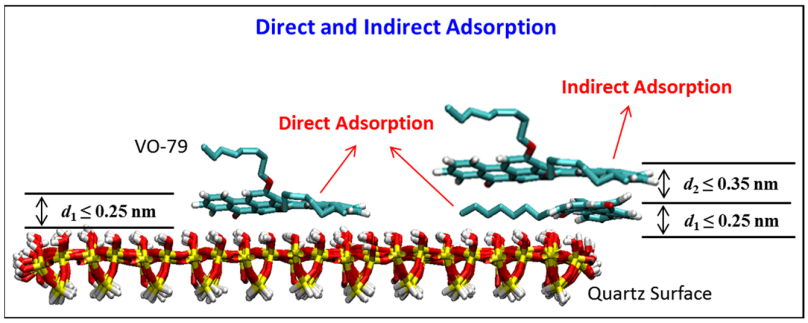

Figure 4. Schematic for direct and indirect adsorption behaviors defined in this work.

Using this criterion, the averaged minimum distance between quartz surfaces and the PACs of all directly adsorbed VO-79 is plotted against time in Figure 3c for the systems in heptane and in Figure 3d for the systems in toluene. Comparing with Figure 3a–b, the fluctuations at 323 and 373 K in Figure 3c–d are smaller, and their final equilibrium values are the same as the others at higher temperatures. Moreover, most systems took longer to reach equilibrium in toluene, than in heptane, indicating that the adsorption of VO-79 onto quartz surface was faster in heptane because of its poorer solubility.[29,70]

The number of VO-79 molecules with different adsorption modes at the end stage of the simulations (80–100 ns) were recorded and plotted in Figure 5a. It can be seen that almost all 24 VO-79 were adsorbed at the end, and the total amount of adsorption was insensitive to solvent or temperature. However, the number of VO-79 with direct adsorption increased markedly with rising temperature in both heptane and toluene, while the VO-79 in indirect form decreased accordingly. At 323K, the numbers of directly and indirectly adsorbed VO-79 were almost equal, while direct adsorption was

more dominant at higher temperatures. The maximum and average rates of direct adsorption are shown in Figure 5b at different temperatures (see Section S4 of SI for calculation details). In both heptane and toluene, the maximum and average rates of direct adsorption increased significantly with the rising temperature.

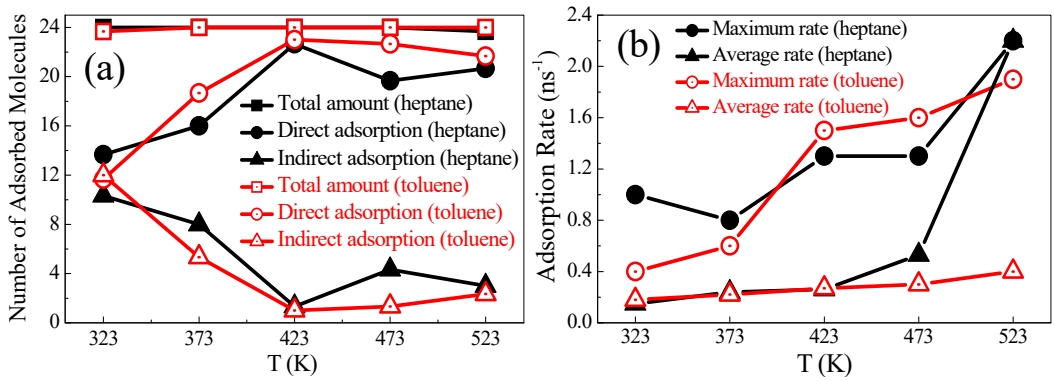

Figure 5. (a) Number of total, directly and indirectly adsorbed VO-79 molecules on quartz surface at the end stage of simulations, and (b) maximum and average rates of VO-79 adsorption in direct form, in heptane and toluene under different temperature conditions.

3.2. Characterization of Adsorbed Layers

In order to better understand the structure of adsorbed layers, the effective thickness of VO-79 layers adsorbed on quartz surfaces was evaluated (see Section S5 of SI for details of the calculation), and plotted in Figure 6, including the thicknesses on the left and right surfaces and their sum (total thickness). At 323 K, the maximum thickness was 4.20 nm in heptane (on the left surface) and 2.98 nm in toluene (on the left surface). These values are slightly smaller than the measured thickness of

asphaltene layers (6.2–8.7 nm) adsorbed from xylene onto a hydrophilic silica surface in experiments at 298 K.[18] With increasing temperature, the total thickness gradually decreased from 6.67 to 4.48 nm in heptane and from 5.71 to 4.46 nm in toluene. Since the total number of adsorbed VO-79 was insensitive to temperature (Figure 5a), the results indicate that raising temperature caused the adsorbed VO-79 to distribute more uniformly over the quartz surface. Furthermore, while the total thickness in toluene was clearly smaller than that in heptane at low temperatures (323 and 373 K), they were almost the same at high temperatures (423, 473 and 523 K). The results suggest that the VO-79 molecules adsorbed on quartz surface from aromatic solvents can distribute more uniformly than those from aliphatic solvents, but the effect of solvent on the morphology of adsorbed VO-79 fades with increasing temperature.

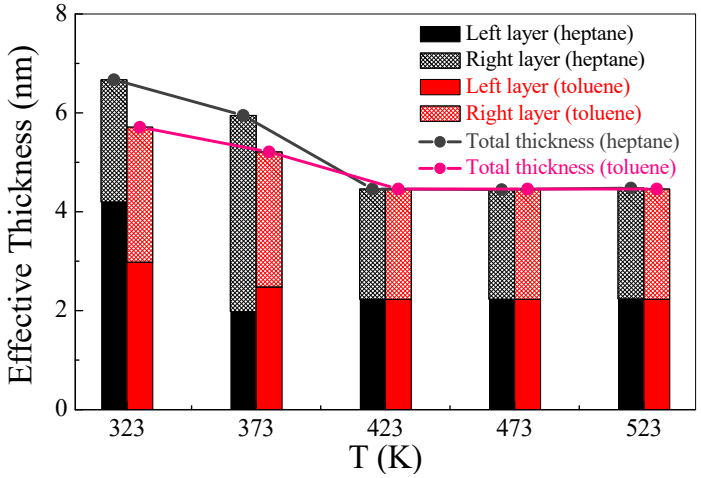

Figure 6. Effective thickness of the adsorbed VO-79 layers (nm) on quartz surfaces.

To further characterize the structure of the adsorbed layers, quantitative analysis on the orientation of PAC planes of the adsorbed VO-79 relative to the quartz surfaces was

311 conducted by computing the cosine of angle θ (cosθ) between them (see Figure 7a).
312 Angle θ can vary from 0° to 90°, thus cosθ is in the range of 0 to 1. When cosθ is less
313 than 0.2, the plane of VO-79 is considered to be perpendicular to the surface. When
314 cosθ is more than 0.9, the plane is considered parallel to the surface. Between these two
315 limits, the plane is considered to be in the slant state. The distributions of cosθ for the
316 PAC planes of VO-79 with direct and indirect adsorptions are plotted in Figure 7. There
317 is no molecule distributed in the range of 0–0.2, indicating no VO-79 presenting
318 perpendicular configuration to the quartz surface in either solvents. For system H323 in
319 heptane (Figure 7a), cosθ is mainly distributed in the range of 0.6–0.9, which reveals
320 that the VO-79 molecules tended to be slant to the surface at 323 K, especially with
321 indirect adsorption. However, with increasing temperature, cosθ has an increasing
322 probability of being in the range of 0.9−1, and 80% of the VO-79 molecules are in this
323 range at 473 and 523 K. This result suggests that at high temperature the VO-79
324 molecules preferred a parallel configuration. By comparison, in toluene (Figure 7b),
325 cosθ of VO-79 with both adsorption modes has a narrower distribution (0.7–1), with a
326 few molecules in a slant configuration (0.7–0.9) but more taking a parallel configuration
327 (0.9–1) as the temperature grows.
328

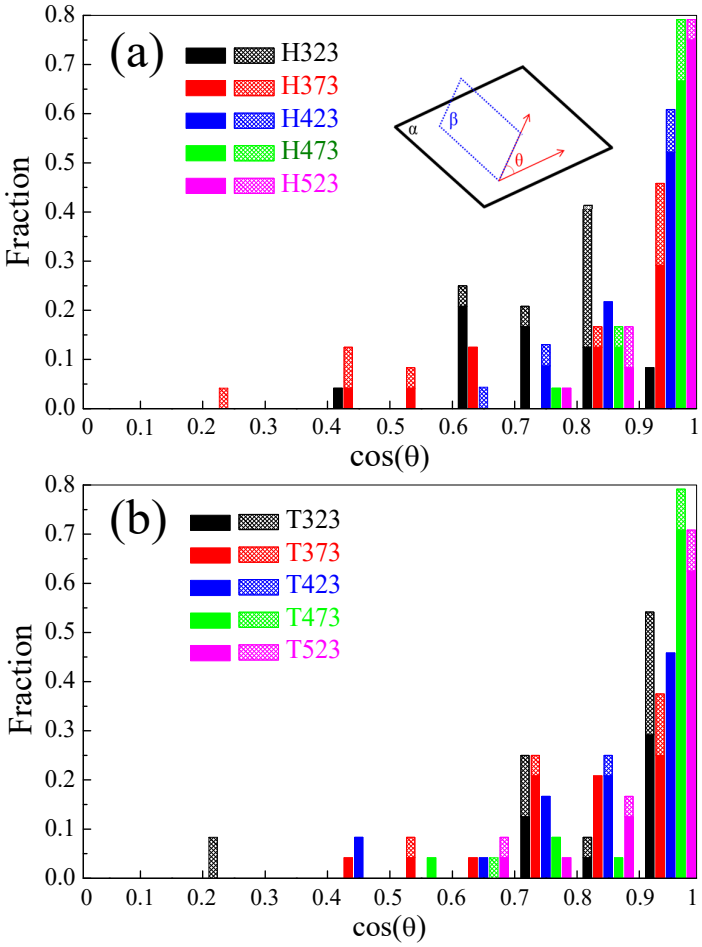

Figure 7. Distribution of cosine of angle θ (cosθ) between PAC plane of the adsorbed VO-79 molecules and quartz surfaces in (a) heptane and (b) toluene under different temperature conditions, averaged over the last 5 ns of the simulations. Inset: schematic depiction of the calculation of cosθ between planes α and β, which are respectively the plane of quartz surface and the PAC plane of VO-79 adsorbed on the surface. Solid columns correspond to the number of molecules in direct adsorption while shaded columns correspond to the number of molecules in indirect adsorption.

3.3. Energetics Analyses

To understand the forces driving VO-79 adsorption on quartz as the temperature

increases, energetics analyses were performed. The changes in van der Waals (ΔE_{vdW}) and electrostatic (ΔE_{elec}) interaction energies between quartz and VO-79, and between quartz and solvents are plotted in Figure 8, along with the change in free energy of solvation (ΔG_{solv}) of VO-79 (see Section S6 in SI) calculated based on the solvent accessible surface area (SASA).[71] From Figure 8, it is clear that in all systems, ΔE_{vdW} and ΔE_{elec} between quartz and VO-79 are negative, indicating that both types of interactions are beneficial to the adsorption of VO-79. However, the electrostatic interaction contributes only a minor portion compared to the vdW interaction which appears to be the dominating force for adsorption under all temperature conditions. ΔG_{solv} is also negative in all systems, and the values are comparable in magnitude to the electrostatic interactions, providing another driving force for the adsorption. More importantly, the vdW interaction between quartz and VO-79 is significantly enhanced with increasing temperature: the magnitude of ΔE_{vdW} at 523K is almost twice that at 323K, in both heptane and toluene. Such significant increase is not observed in ΔE_{elec} or ΔG_{solv}. As VO-79 moved to the vicinity of the quartz surfaces and replaced the solvent molecules there, both ΔE_{vdW} and ΔE_{elec} between quartz and solvents are positive, resisting VO-79 adsorption on the surface. However, such positive ΔE are smaller in magnitude compared with the negative ΔE between quartz and VO-79, which demonstrates that VO-79 adsorption on the quartz surface is energetically favored compared with solvent adsorption.

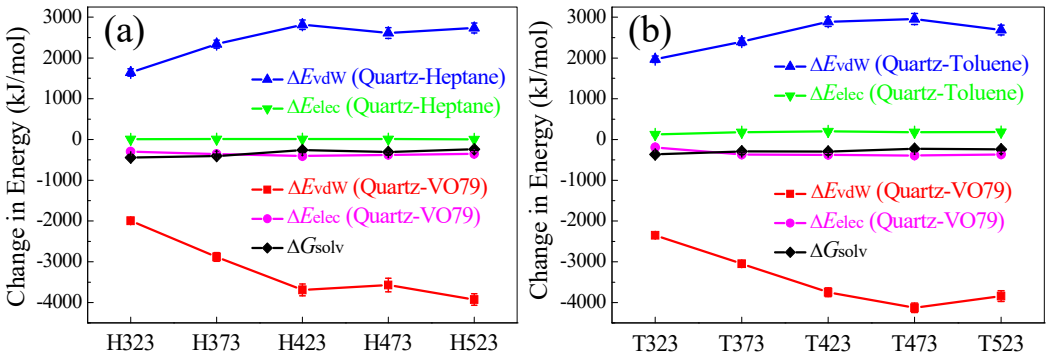

Figure 8. Change in interaction energy (ΔE) between quartz and VO-79, and between quartz and solvents in (a) heptane and (b) toluene, along with the change in free energy of solvation (ΔG_{solv}) of VO-79.

3.4. AFM Imaging of Adsorbed Layers

The morphologies of VO-79 adsorbed on silica surface were characterized at different temperatures using AFM imaging, and the images are shown in Figure 9. In heptane, at 298 K (Figure 9a), the adsorbed VO-79 formed some large aggregates over the silica surface with the height of 35–50 nm, and the diameter of the largest aggregate was about 1.0 μm (Table 2). At 323 K (Figure 9b), these large aggregates significantly broke down, as evidenced by the decrease in both height and maximum diameter of aggregates, which were measured to be in the range of 5–30 nm and about 0.5 μm, respectively. When further raising temperature to 363 K (Figure 9c), the VO-79 aggregates became even smaller with the height of around 1.5 nm and the maximum diameter of about 0.2 μm, displaying a uniform distribution over the substrate surface. Similar phenomena were also observed in toluene. For example, the height of the VO-79 aggregates formed at 298, 323, and 363 K was respectively in the range of 10–

23 nm (Figure 9d), 2–10 nm (Figure 9e), and around 1.0 nm (Figure 9f), while the maximum diameter of the aggregates was about 0.6, 0.3, and 0.1 μm, respectively. These experimental results show that increasing temperature can reduce the size of the adsorbed VO-79 aggregates on the silica surface, which is consistent with the earlier report,[34] and enable the adsorbed molecules to distribute more uniformly over the substrate surface regardless of the type of solvent. Moreover, the formed VO-79 aggregates on the surface were smaller in good solvent toluene than in poor solvent heptane under all temperature conditions. Although the temperature range applied in experiments is different from the MD simulation due to the limitation of the experiment equipment available, this measured trend confirmed the validity of the observations in the MD simulations, such as final configurations (Figure 2), minimum distance (Figure 3) and effective thickness (Figure 6).

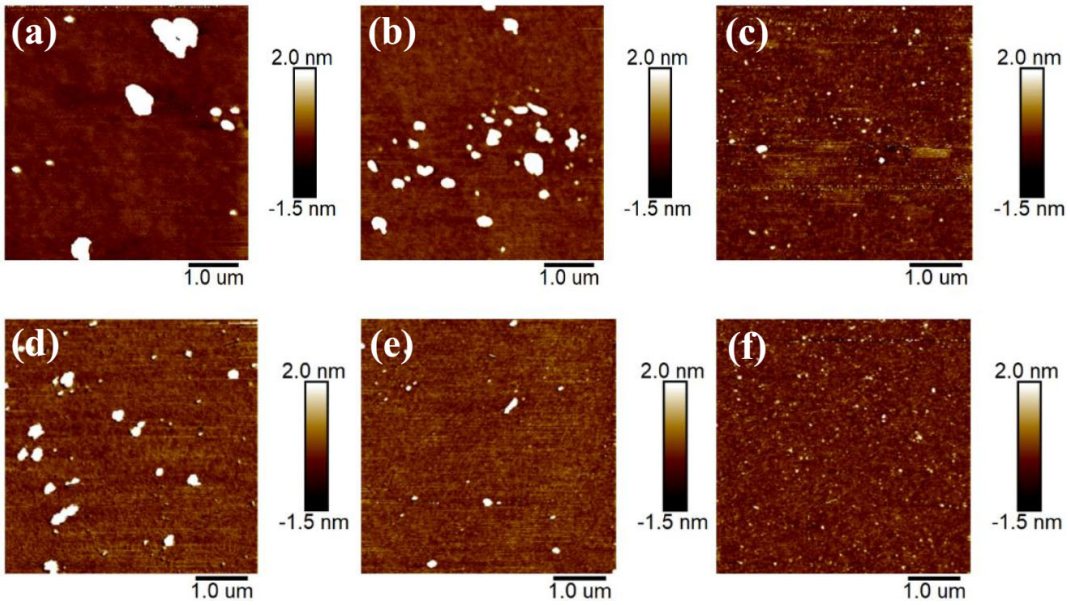

Figure 9. Topographic AFM images (5 × 5 μm) of VO-79 adsorbed on the silica surface

in heptane (upper panel) and toluene (bottom panel) at (a,d) 298 K, (b,e) 323 K and (c,f) 363 K.

Table 2. Height and Maximum Diameter of the VO-79 Aggregates

temperature	height (nm)		maximum diameter (μm)	
	in heptane	in toluene	in heptane	in toluene
298 K	35–50	10–23	1.0	0.6
323 K	5–30	2–10	0.5	0.3
363 K	1.5	1.0	0.2	0.1

3.5. Discussion

To our knowledge, this work presents the first set of MD simulations that systematically investigate the effect of temperature on the adsorption of PAHs onto mineral surfaces. Two modes of adsorption, direct and indirect, were observed in the adsorption process, which were fitted and modelled in previous experimental studies.[9,18] Earlier studies have shown that for asphaltenes, their initial size (i.e., molecular weight) and the resulting size of the aggregates can significantly affect their ability to interact with the active sites of mineral surfaces[4,72]. Increasing temperature can disrupt the associations that hold the PAH molecules together, thus breaking the aggregates into smaller ones,[34] resulting in less buried functional groups and more likelihood to interact with the binding sites on the surfaces.[17] In our previous work, the adsorption of asphaltenes on mica surface was identified as being mainly controlled by the diffusion of asphaltene aggregates from the bulk solution to the surface,[11] and decreasing the size of the aggregates will increase their rate of diffusion.[73-75] In other words, increasing

414 temperature can also accelerate the adsorption of PAHs on mineral surfaces by
415 providing faster rate of diffusion.[76] This result is consistent with the observations in our
416 simulations and AFM imaging where the adsorption rates increased with rising
417 temperature and direct adsorption became more dominant at high temperatures,
418 enabling VO-79 molecules to distribute more uniformly over the quartz surface. On the
419 other hand, we did not observe a decrease in the adsorption amount with the increase of
420 temperature as reported in some literatures,[30,31,35-37] as almost all 24 molecules were
421 adsorbed on the quartz surface in the final stage of the simulations. It should be pointed
422 out that past studies also exist which claimed that temperature did not affect the overall
423 adsorption of asphaltenes on solid surfaces and was only important during short reaction
424 times.[4] The insensitivity of overall adsorption found in our work might be due to the
425 relatively high surface silanol density (about 7.2 OH per nm^2) on the quartz model,
426 which enabled a higher chemical activity. In this regime, our results suggest that
427 temperature affects the kinetics and mode of adsorption, while having little effect on the
428 amount of adsorption.[38]

429 The type of solvent also influences the adsorbed structures. Previous study showed
430 that,[18] when heptane is progressively added into an asphaltene solution in xylene, the
431 adsorbed asphaltene layer changed from a monolayer structure (with direct adsorption)
432 to a multilayer one (with indirect adsorption) once the bulk flocculation threshold was
433 exceeded. This phenomenon is consistent with the results in our simulations that the
434 total thicknesses in heptane are larger than those in toluene at low temperatures. It is
435 interesting, however, to note that when the temperature is sufficiently high, the
436 differences caused by different solvents diminish, and the adsorbed layers are uniform
437 regardless of the solvent type.

438 Together with our previous studies,[11,12,49] the results reported here have generated a

more complete picture of PAHs adsorption on mineral surfaces under different external environmental conditions. The mechanistic understanding brought by our series of studies can provide useful insights into modulating the PAH adsorption on mineral surfaces in practical applications such as improving oil recovery and avoiding surface fouling in industrial processes. However, ~~as we all know,~~it should be recognized that real crude oil is a complex mixture and there can be large variations in the composition depending on its source. In this work, we used a very simple representation of the asphaltene and the oil phase, which is unavoidably associated with some limitations. For example, in a real oil sample, the structures of asphaltenes from different sources ~~will~~ may be different, which ~~will~~ can lead to different adsorption behaviors on mineral surfaces. Also, there are some aliphatic components in real oil, such as dodecane, in which asphaltenes have poor solubility, and this can result~~ing~~ in a rapid adsorption. Therefore, in the future work, ~~the adsorption behavior of~~ different PAH molecules in a variety of mixed solvents may be more suitable to simulate the ~~interactions~~ adsorption behavior ~~between~~ of asphaltenes in real crude oil ~~and~~ on minerals.

4. CONCLUSIONS

A series of MD simulations were carried out to probe the adsorption of polycyclic aromatic hydrocarbons on quartz surface, using VO-79 as a model compound. Two different solvents, heptane and toluene, and five different temperatures ranging from 323 K to 523 K were applied to explore the influence of these external conditions. Our simulations demonstrated that temperature had a great influence on the adsorption, including adsorption mode and rate. With rising temperature, the adsorption rate increased whereas the total amount of stably adsorbed VO-79 molecules hardly changed. The adsorption mode had a strong dependence on the temperature. At 323K,

approximately half of the adsorbed VO-79 formed a monolayer with direct adsorption and the other half were in an aggregated form with indirect adsorption. A transition from indirect to direct adsorption was observed as temperature increased, and nearly 90% of VO-79 molecules were adsorbed in direct form at 523K. Detailed structural characterization revealed that the total thicknesses of adsorbed layers gradually decreased with the increase of temperature, suggesting more uniform distribution of the molecules over the quartz surface. In addition, and the effect of solvent on the morphology of adsorbed VO-79 faded as temperature rose. AFM imaging confirmed the observed trend in the MD simulations, showing smaller and more uniformly distributed VO-79 aggregates adsorbed on the silica surface with increasing temperature. Our results improved the mechanistic understanding of PAH adsorption on mineral surfaces, with useful implications on better modulating the related interfacial processes where PAHs are involved in practical applications.

■ ASSOCIATED CONTENT

Supporting Information

The Supporting Information is available free of charge on the ACS Publications website at DOI:

Initial configuration, minimum distance, calculations of the direct adsorption rates and the effective thickness of adsorbed VO-79 layers, and free energy of solvation (PDF)

■ AUTHOR INFORMATION

Corresponding Authors

*(H.Z.) Phone: +1-780-492-1044; E-mail: hongbo.zeng@ualberta.ca.

*(T.T.) Phone: +1-780-492-5467; E-mail: tian.tang@ualberta.ca.

ORCID

Tu Lan: 0000-0002-9877-2636

Tian Tang: 0000-0002-2387-3571

Hongbo Zeng: 0000-0002-1432-5979

Notes

The authors declare no competing financial interest.

■ ACKNOWLEDGMENTS

We acknowledge the computing resources and technical support from Western Canada Research Grid (WestGrid). Financial support from the Natural Science and Engineering Research Council (NSERC) of Canada, and the Future Energy Systems under the Canada First Research Excellence Fund and the Canada Research Chairs Program is gratefully acknowledged.

■ REFERENCES

(1) Qu, X.; Liu, P.; Zhu, D. Enhanced sorption of polycyclic aromatic hydrocarbons to tetra-alkyl ammonium modified smectites via cation−π interactions. *Environ. Sci. Technol.* **2008,** *42*, 1109-1116.

(2) Lamichhane, S.; Bal Krishna, K. C.; Sarukkalige, R. Polycyclic aromatic hydrocarbons (PAHs) removal by sorption: A review. *Chemosphere* **2016,** *148*, 336-353.

(3) Morrow, N. R.; Mason, G. Recovery of oil by spontaneous imbibition. *Curr. Opin. Colloid Interface Sci.* **2001,** *6*, 321-337.

(4) Adams, J. J. Asphaltene adsorption, a literature review. *Energy Fuels* **2014,** *28*, 2831-2856.

(5) Jiang, T.; Hirasaki, G. J.; Miller, C. A.; Ng, S. Wettability alteration of clay in solid-stabilized emulsions. *Energy Fuels* **2011,** *25*, 2551-2558.

(6) Zhang, L.; Lu, X.; Liu, X.; Yang, K.; Zhou, H. Surface wettability of basal surfaces of clay minerals: Insights from molecular dynamics simulation. *Energy Fuels* **2016,** *30*, 149-160.

(7) Kim, S.; Marcano, M. C.; Becker, U. Mechanistic study of wettability changes on calcite by molecules containing a polar hydroxyl functional group and nonpolar benzene rings. *Langmuir* **2019,** *35*, 2527-2537.

(8) Dudášová, D.; Simon, S.; Hemmingsen, P. V.; Sjöblom, J. Study of asphaltenes adsorption onto different minerals and clays: Part 1. Experimental adsorption with UV depletion detection. *Colloids Surf., A* **2008,** *317*, 1-9.

(9) de la Cruz, J. L. M.; Castellanos-Ramírez, I. V.; Ortiz-Tapia, A.; Buenrostro-González, E.; Durán-Valencia, C. d. l. A.; López-Ramírez, S. Study of monolayer to multilayer adsorption of asphaltenes on reservoir rock minerals. *Colloids Surf., A* **2009,** *340*, 149-154.

(10) Wang, S.; Liu, Q.; Tan, X.; Xu, C.; Gray, M. R. Study of asphaltene adsorption on kaolinite by X-ray photoelectron spectroscopy and time-of-flight secondary ion mass spectroscopy. *Energy Fuels* **2013,** *27*, 2465-2473.

(11) Natarajan, A.; Kuznicki, N.; Harbottle, D.; Masliyah, J.; Zeng, H.; Xu, Z. Understanding mechanisms of asphaltene adsorption from organic solvent on mica. *Langmuir* **2014,** *30*, 9370-9377.

(12) Huang, J.; Stoyanov, S. R.; Zeng, H. A comparison study on adsorption and interaction behaviors of diluted bitumen and conventional crude oil on model mineral surface. *Fuel* **2019,** *253*, 383-391.

(13) Dudášová, D.; Flåten, G. R.; Sjöblom, J.; Øye, G. Study of asphaltenes adsorption onto different minerals and clays: Part 2. Particle characterization and suspension stability. *Colloids Surf., A* **2009,** *335*, 62-72.

(14) Xing, C.; Hilts, R. W.; Shaw, J. M. Sorption of athabasca vacuum residue constituents on synthetic mineral and process equipment surfaces from mixtures with pentane. *Energy Fuels* **2010,** *24*, 2500-2513.

(15) Saraji, S.; Goual, L.; Piri, M. Adsorption of asphaltenes in porous media under flow conditions. *Energy Fuels* **2010,** *24*, 6009-6017.

(16) Guo, M.; Tan, Y.; Wang, L.; Hou, Y. Diffusion of asphaltene, resin, aromatic and saturate components of asphalt on mineral aggregates surface: molecular dynamics simulation. *Road Mater. Pavement* **2017,** *18*, 149-158.

(17) Abudu, A.; Goual, L. Adsorption of crude oil on surfaces using quartz crystal microbalance with dissipation (QCM-D) under flow conditions. *Energy Fuels* **2009,** *23*, 1237-1248.

(18) Jouault, N.; Corvis, Y.; Cousin, F.; Jestin, J.; Barré, L. Asphaltene adsorption mechanisms on the local scale probed by neutron reflectivity: Transition from monolayer to multilayer growth above the flocculation threshold. *Langmuir* **2009,** *25*, 3991-3998.

(19) Zahabi, A.; Gray, M. R.; Dabros, T. Kinetics and properties of asphaltene adsorption on surfaces. *Energy Fuels* **2012,** *26*, 1009-1018.

(20) Zhao, H.; Long, J.; Masliyah, J. H.; Xu, Z. Effect of divalent cations and surfactants on silica-bitumen interactions. *Ind. Eng. Chem. Res.* **2006,** *45*, 7482-7490.

(21) Farooq, U.; Sjöblom, J.; Øye, G. Desorption of asphaltenes from silica-coated quartz crystal surfaces in low saline aqueous solutions. *J. Dispersion Sci. Technol.* **2011,** *32*, 1388-1395.

(22) Saraji, S.; Goual, L.; Piri, M. Dynamic adsorption of asphaltenes on quartz and calcite packs in the presence of brine films. *Colloids Surf., A* **2013,** *434*, 260-267.

(23) Underwood, T.; Erastova, V.; Cubillas, P.; Greenwell, H. C. Molecular dynamic simulations of montmorillonite–organic interactions under varying salinity: An insight into enhanced oil recovery. *J. Phys. Chem. C* **2015,** *119*, 7282-7294.

(24) Gonzalez, V.; Taylor, S. E. Asphaltene adsorption on quartz sand in the presence of pre-adsorbed water. *J. Colloid Interface Sci.* **2016,** *480*, 137-145.

(25) Khanniche, S.; Mathieu, D.; Barthet, C.; Pereira, F.; Hairault, L. Molecular dynamics simulation of gaseous nitroaromatic compounds interacting with silica surfaces under various humidity conditions. *Appl. Surf. Sci.* **2018,** *455*, 533-542.

(26) Higaki, Y.; Hatae, K.; Ishikawa, T.; Takanohashi, T.; Hayashi, J.-i.; Takahara, A. Adsorption and desorption behavior of asphaltene on polymer-brush-immobilized surfaces. *ACS Appl. Mater. Interfaces* **2014,** *6*, 20385-20389.

(27) Hmoudah, M.; Nassar, N. N.; Vitale, G.; El-Qanni, A. Effect of nanosized and surface-structural-modified nano-pyroxene on adsorption of violanthrone-79. *RSC Adv.* **2016,** *6*, 64482-64493.

(28) Jena, N. K.; Lyne, Å. L.; Arul Murugan, N.; Ågren, H.; Birgisson, B. Atomic level simulations of the interaction of asphaltene with quartz surfaces: role of chemical modifications and aqueous environment. *Mater. Struct.* **2016,** *50*, 99.

(29) Yarranton, H. W.; Alboudwarej, H.; Jakher, R. Investigation of asphaltene association with vapor pressure osmometry and interfacial tension measurements. *Ind. Eng. Chem. Res.* **2000,** *39*, 2916-2924.

(30) Alboudwarej, H.; Pole, D.; Svrcek, W. Y.; Yarranton, H. W. Adsorption of asphaltenes on metals. *Ind. Eng. Chem. Res.* **2005,** *44*, 5585-5592.

(31) Nassar, N. N. Asphaltene adsorption onto alumina nanoparticles: Kinetics and thermodynamic studies. *Energy Fuels* **2010,** *24*, 4116-4122.

(32) Acevedo, S.; García, L. A.; Rodríguez, P. Changes of diameter distribution with temperature measured for asphaltenes and their fractions A1 and A2. Impact of these measurements in colloidal and solubility issues of asphaltenes. *Energy Fuels* **2012,** *26*, 1814-1819.

(33) Carlos da Silva Ramos, A.; Haraguchi, L.; Notrispe, F. R.; Loh, W.; Mohamed, R. S. Interfacial and colloidal behavior of asphaltenes obtained from Brazilian crude oils. *J. Petrol. Sci. Eng.* **2001,** *32*, 201-216.

(34) Pierre, C.; Barré, L.; Pina, A.; Moan, M. Composition and heavy oil rheology. *Oil Gas Sci. Technol.* **2004,** *59*, 489-501.

(35) Cortés, F. B.; Mejía, J. M.; Ruiz, M. A.; Benjumea, P.; Riffel, D. B. Sorption of asphaltenes onto nanoparticles of nickel oxide supported on nanoparticulated silica gel. *Energy Fuels* **2012,** *26*, 1725-1730.

(36) Franco, C.; Patiño, E.; Benjumea, P.; Ruiz, M. A.; Cortés, F. B. Kinetic and thermodynamic equilibrium of asphaltenes sorption onto nanoparticles of nickel oxide supported on nanoparticulated

alumina. *Fuel* **2013,** *105*, 408-414.
(37) Nassar, N. N.; Montoya, T.; Franco, C. A.; Cortés, F. B.; Pereira-Almao, P. A new model for describing the adsorption of asphaltenes on porous media at a high pressure and temperature under flow conditions. *Energy Fuels* **2015,** *29*, 4210-4221.
(38) Franco, C. A.; Giraldo, J.; Ruiz, M. A.; Rojano, B. A.; Cortes, F. B. Kinetic and thermodynamic equilibrium of asphaltenes sorption onto formation rock: evaluation of the wash in the adsorptive properties. *Dyna* **2012,** *79*, 81-89.
(39) Kuznicki, T.; Masliyah, J. H.; Bhattacharjee, S. Aggregation and partitioning of model asphaltenes at toluene−water interfaces: Molecular dynamics simulations. *Energy Fuels* **2009,** *23*, 5027-5035.
(40) Mikami, Y.; Liang, Y.; Matsuoka, T.; Boek, E. S. Molecular dynamics simulations of asphaltenes at the oil–water interface: From nanoaggregation to thin-film formation. *Energy Fuels* **2013,** *27*, 1838-1845.
(41) Gao, F.; Xu, Z.; Liu, G.; Yuan, S. Molecular dynamics simulation: The behavior of asphaltene in crude oil and at the oil/water interface. *Energy Fuels* **2014,** *28*, 7368-7376.
(42) Teklebrhan, R. B.; Ge, L.; Bhattacharjee, S.; Xu, Z.; Sjöblom, J. Initial partition and aggregation of uncharged polyaromatic molecules at the oil–water interface: A molecular dynamics simulation study. *J. Phys. Chem. B* **2014,** *118*, 1040-1051.
(43) Liu, J.; Zhao, Y.; Ren, S. Molecular dynamics simulation of self-aggregation of asphaltenes at an oil/water interface: Formation and destruction of the asphaltene protective film. *Energy Fuels* **2015,** *29*, 1233-1242.
(44) Jian, C.; Zeng, H.; Liu, Q.; Tang, T. Probing the adsorption of polycyclic aromatic compounds onto water droplets using molecular dynamics simulations. *J. Phys. Chem. C* **2016,** *120*, 14170-14179.
(45) Jian, C.; Liu, Q.; Zeng, H.; Tang, T. Effect of model polycyclic aromatic compounds on the coalescence of water-in-oil emulsion droplets. *J. Phys. Chem. C* **2017,** *121*, 10382-10391.
(46) Wu, G.; He, L.; Chen, D. Sorption and distribution of asphaltene, resin, aromatic and saturate fractions of heavy crude oil on quartz surface: Molecular dynamic simulation. *Chemosphere* **2013,** *92*, 1465-1471.
(47) Zhu, X.; Chen, D.; Wu, G. Insights into asphaltene aggregation in the Na-montmorillonite interlayer. *Chemosphere* **2016,** *160*, 62-70.
(48) Xiong, Y.; Cao, T.; Chen, Q.; Li, Z.; Yang, Y.; Xu, S.; Yuan, S.; Sjöblom, J.; Xu, Z. Adsorption of a polyaromatic compound on silica surfaces from organic solvents studied by molecular dynamics simulation and AFM imaging. *J. Phys. Chem. C* **2017,** *121*, 5020-5028.
(49) Lan, T.; Zeng, H.; Tang, T. Understanding adsorption of violanthrone-79 as a model asphaltene compound on quartz surface using molecular dynamics simulations. *J. Phys. Chem. C* **2018,** *122*, 28787-28796.
(50) Zhu, X.; Chen, D.; Zhang, Y.; Wu, G. Insights into the oil adsorption and cyclodextrin extraction process on rough silica surface by molecular dynamics simulation. *J. Phys. Chem. C* **2018,** *122*, 2997-3005.

(51) Xiong, Y.; Li, Z.; Cao, T.; Xu, S.; Yuan, S.; Sjöblom, J.; Xu, Z. Synergistic adsorption of polyaromatic compounds on silica surfaces studied by molecular dynamics simulation. *J. Phys. Chem. C* **2018,** *122*, 4290-4299.

(52) Bai, Y.; Sui, H.; Liu, X.; He, L.; Li, X.; Thormann, E. Effects of the N, O, and S heteroatoms on the adsorption and desorption of asphaltenes on silica surface: A molecular dynamics simulation. *Fuel* **2019,** *240*, 252-261.

(53) Hair, M. L.; Hertl, W. Adsorption on hydroxylated silica surfaces. *J. Phys. Chem.* **1969,** *73*, 4269-4276.

(54) Parida, S. K.; Dash, S.; Patel, S.; Mishra, B. K. Adsorption of organic molecules on silica surface. *Adv. Colloid Interface Sci.* **2006,** *121*, 77-110.

(55) Rimola, A.; Costa, D.; Sodupe, M.; Lambert, J.-F.; Ugliengo, P. Silica surface features and their role in the adsorption of biomolecules: Computational modeling and experiments. *Chem. Rev.* **2013,** *113*, 4216-4313.

(56) Gallas, J.-P.; Goupil, J.-M.; Vimont, A.; Lavalley, J.-C.; Gil, B.; Gilson, J.-P.; Miserque, O. Quantification of water and silanol species on various silicas by coupling IR spectroscopy and in-situ thermogravimetry. *Langmuir* **2009,** *25*, 5825-5834.

(57) Jian, C.; Poopari, M. R.; Liu, Q.; Zerpa, N.; Zeng, H.; Tang, T. Reduction of water/oil interfacial tension by model asphaltenes: The governing role of surface concentration. *J. Phys. Chem. B* **2016,** *120*, 5646-5654.

(58) Jian, C.; Poopari, M. R.; Liu, Q.; Zerpa, N.; Zeng, H.; Tang, T. Mechanistic understanding of the effect of temperature and salinity on the water/toluene interfacial tension. *Energy Fuels* **2016,** *30*, 10228-10235.

(59) Jian, C.; Liu, Q.; Zeng, H.; Tang, T. A molecular dynamics study of the effect of asphaltenes on toluene/water interfacial tension: Surfactant or solute? *Energy Fuels* **2018,** *32*, 3225-3231.

(60) Lan, T.; Zeng, H.; Tang, T. Molecular dynamics study on the mechanism of graphene oxide to destabilize oil/water emulsion. *J. Phys. Chem. C* **2019,** *123*, 22989-22999.

(61) Pronk, S.; Páll, S.; Schulz, R.; Larsson, P.; Bjelkmar, P.; Apostolov, R.; Shirts, M. R.; Smith, J. C.; Kasson, P. M.; van der Spoel, D.; Hess, B.; Lindahl, E. GROMACS 4.5: A high-throughput and highly parallel open source molecular simulation toolkit. *Bioinformatics* **2013,** *29*, 845-854.

(62) Abraham, M. J.; Murtola, T.; Schulz, R.; Páll, S.; Smith, J. C.; Hess, B.; Lindahl, E. GROMACS: High performance molecular simulations through multi-level parallelism from laptops to supercomputers. *SoftwareX* **2015,** *1-2*, 19-25.

(63) Bussi, G.; Donadio, D.; Parrinello, M. Canonical sampling through velocity rescaling. *J. Chem. Phys.* **2007,** *126*, 014101.

(64) Parrinello, M.; Rahman, A. Polymorphic transitions in single crystals: A new molecular dynamics method. *J. Appl. Phys.* **1981,** *52*, 7182-7190.

(65) Hess, B. P-LINCS: A parallel linear constraint solver for molecular simulation. *J. Chem. Theory*

Comput. **2008,** *4*, 116-122.
(66) Darden, T.; York, D.; Pedersen, L. Particle mesh Ewald: An N·log (N) method for Ewald sums in large systems. *J. Chem. Phys.* **1993,** *98*, 10089-10092.
(67) Essmann, U.; Perera, L.; Berkowitz, M. L.; Darden, T.; Lee, H.; Pedersen, L. G. A smooth particle mesh Ewald method. *J. Chem. Phys.* **1995,** *103*, 8577-8593.
(68) Humphrey, W.; Dalke, A.; Schulten, K. VMD: Visual molecular dynamics. *J. Mol. Graph.* **1996,** *14*, 33-38.
(69) Jian, C.; Tang, T.; Bhattacharjee, S. Probing the effect of side-chain length on the aggregation of a model asphaltene using molecular dynamics simulations. *Energy Fuels* **2013,** *27*, 2057-2067.
(70) Speight, J. G.; Long, R. B.; Trowbridge, T. D. Factors influencing the separation of asphaltenes from heavy petroleum feedstocks. *Fuel* **1984,** *63*, 616-620.
(71) Eisenhaber, F.; Lijnzaad, P.; Argos, P.; Sander, C.; Scharf, M. The double cubic lattice method: Efficient approaches to numerical integration of surface area and volume and to dot surface contouring of molecular assemblies. *J. Comput. Chem.* **1995,** *16*, 273-284.
(72) Marchal, C.; Abdessalem, E.; Tayakout-Fayolle, M.; Uzio, D. Asphaltene diffusion and adsorption in modified NiMo alumina catalysts followed by ultraviolet (UV) spectroscopy. *Energy Fuels* **2010,** *24*, 4290-4300.
(73) Xie, K.; Karan, K. Kinetics and thermodynamics of asphaltene adsorption on metal surfaces: A preliminary study. *Energy Fuels* **2005,** *19*, 1252-1260.
(74) Dudášová, D.; Silset, A.; Sjöblom, J. Quartz crystal microbalance monitoring of asphaltene adsorption/deposition. *J. Dispersion Sci. Technol.* **2008,** *29*, 139-146.
(75) Syunyaev, R. Z.; Balabin, R. M.; Akhatov, I. S.; Safieva, J. O. Adsorption of petroleum asphaltenes onto reservoir rock sands studied by near-infrared (NIR) spectroscopy. *Energy Fuels* **2009,** *23*, 1230-1236.
(76) Kumar, K.; Dao, E.; Mohanty, K. K. AFM study of mineral wettability with reservoir oils. *J. Colloid Interface Sci.* **2005,** *289*, 206-217.

693 **TOC Graphic:**

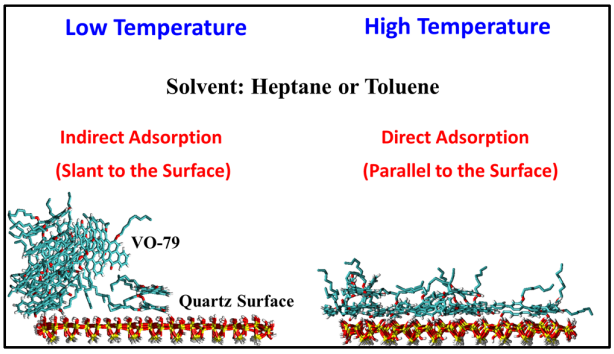

694